Supplementary Information

Mechano-optical analysis of single cells with transparent microcapillary resonators

Alberto Martín-Pérez, Daniel Ramos*, Eduardo Gil-Santos, Sergio García-López, Marina L. Yubero, Priscila M. Kosaka, Álvaro San Paulo, Javier Tamayo and Montserrat Calleja*

Bionanomechanics Lab, Instituto de Micro y Nanotecnología, IMN-CNM (CSIC), Isaac Newton 8 (PTM), E-28760 Tres Cantos, Madrid, Spain.

S1. Device Fabrication

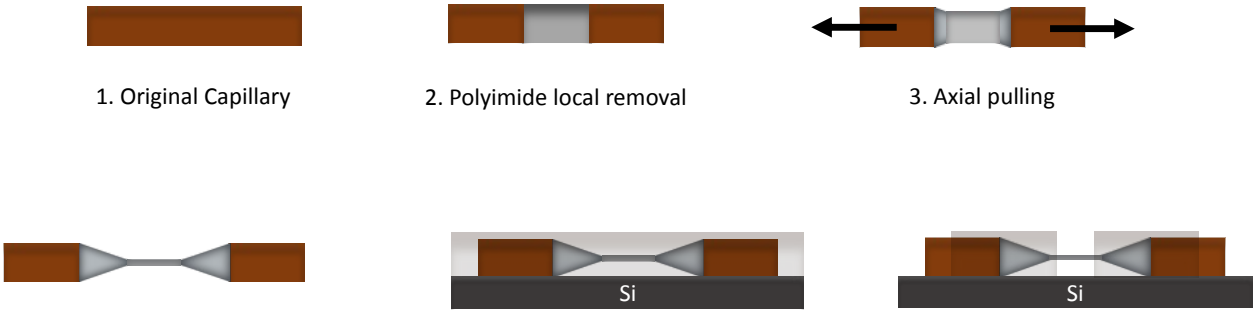

Figure S1. Device fabrication process.

We have used commercially available glass capillaries (350 µm outer diameter, 250 µm inner diameter and 20µm thick polyimide coating, Polymicro Technologies, TSP250350) . In order to reduce the capillary dimensions, we heat the capillary up to the glass melting point while applying a controlled stress. This stretching process sets the final dimeter of the device within a 1 µm precision. The local heating is applied by a controlled flame, which also removes the capping layer by pyrolysis, revealing the transparent glass capillary. Once the polyimide layer is removed, we apply an axial pulling under the microscope until reaching the desired size. We subsequently pattern the clamping SU8 pads by standard cleanroom photolithography process: SU8 spin coating and photolithography (Fig.S1). The whole procedure ends up with a suspended double clamped transparent silica capillary, optical micrograph in Fig.S2a and SEM image in Fig.S2b.

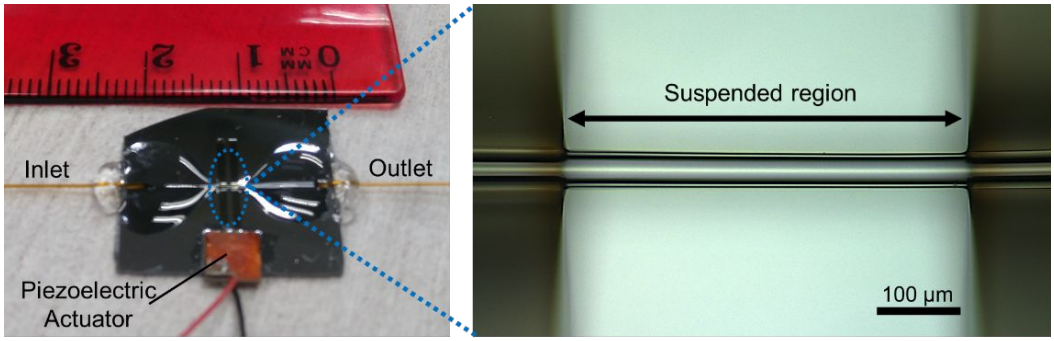

Figure S2. Left. Photograph of the device. **Right**. Optical micrograph of the suspended area

S2. Experimental setup and measurement method

The mechanical displacement of the capillary is optically detected by using a homemade interferometer (Fig.S3). We focus a laser beam on the middle region of the suspended capillary (beam waist ~ 20 μm) and we collect the reflected light by means of a 20X magnification, 0.42 NA objective. The intensity of the collected light is measured by a photodetector (model PDA 10A-EC, Thorlabs, Inc., NJ, USA). The signal provided by the photodetector is split into its AC and DC components. The AC signal contains the information about the displacement of the resonator, while the DC component reveals information about the optical power reflected by the capillary.

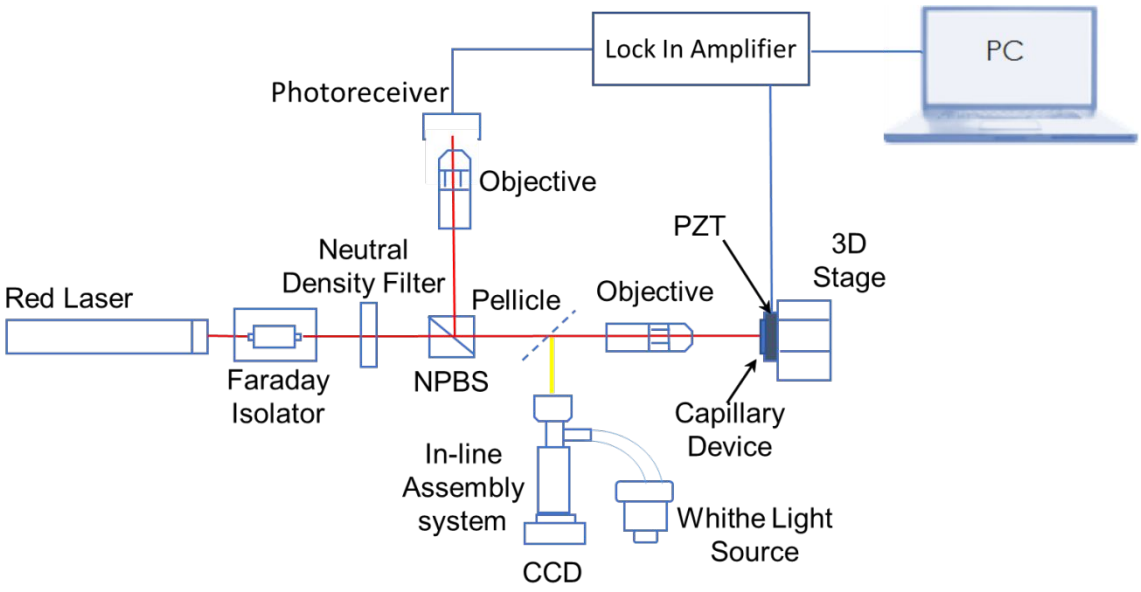

Figure S3. Schematics of the experimental setup.

The microcapillary is mechanically driven by a piezoelectric actuator located on the silicon substrate and by using a lock-in amplifier (model UHFLI-600, Zurich Instruments AG, Switzerland), which also serves for the measurement of the resonance. The lock-in amplifier input signal comes from the photodetector while the output is configured as a sinusoidal electric signal at resonance with an amplitude of 1.5 V and connected to the piezoelectric actuator. In the lock-in amplifier the phase shift is measured in real time using a 2 kHz sampling rate with the demodulator frequency fixed at the resonator's resonance frequency. As the phase presents a linear trend near to the resonance frequency (Fig.S4), phase shift can be used to measure small frequency shifts (< 1kHz). Finally, the phase versus time data are straightforwardly converted to frequency shift versus time signal by setting the mean phase to 0 and multiplying by the slope in the phase vs. frequency linear region (43 $Hz \cdot deg^{-1}$), Fig.S4.

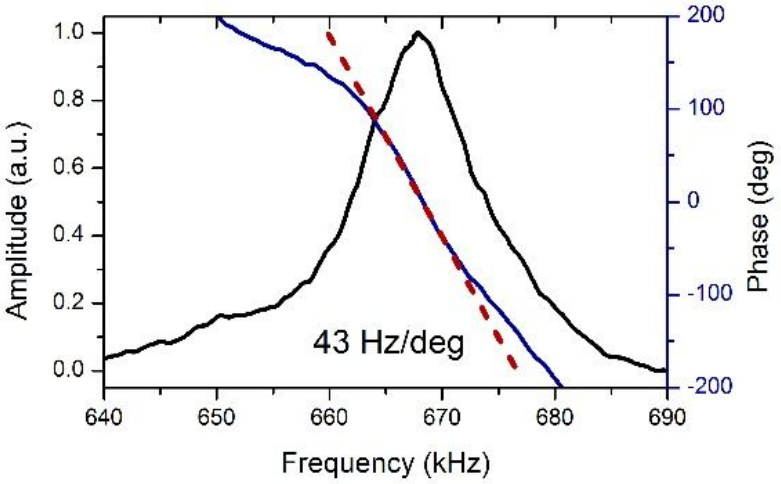

Figure S4. Mechanical Spectrum of the suspended device. Black solid curve represents the normalized amplitude of the signal, the blue solid curve is the phase change, whereas the red dashed line represents the conversion factor Amplitude/Phase.

S3. Sensor Calibration: mass response

The mass sensitivity depends on the inertial mass of the resonator. Thus, it is dependent on the device dimensions, on the relation between the inner and the outer diameter of device and the density of the flowing liquid. Hence, if the density of the inner liquid is changed the resonance frequency (f) shifts following $f = f_0 - R\Delta\rho$. Being f_0 the initial resonance frequency of the resonator (filled with ultra-pure water), R the responsivity ($R = (f_0 V_{in})/2m_0$), V_{in} the volume occupied by the fluid (measured by optical microscopy) and m_0 the mass of the resonator (filled with ultra-pure water). Obtaining m_0 is necessary to convert the data of the frequency shift caused by the flowing particles into the particle mass. We have measured the frequency shift caused by calibration liquids (aqueous solutions of ethanol at different concentrations) and compared this frequency when to that of the same device filled with ultra-pure water at 25° C ($\rho_{water} = 998\ kg/m^3$). The concentrations used for the calibration were: 75% (v/v) ($\Delta\rho = -0.124\ g/mL$), 50% ($\Delta\rho = -0.065 g/mL$) and 25% ($\Delta\rho = -0.027 g/mL$), Fig.S5. By linear fitting of the frequency shift versus the density difference, we can obtain either the density responsivity (-0.11 Hz·mL·µg^{-1}) or the mass of the resonator, that it is of 1.8 µg when filled with ultra-pure water.

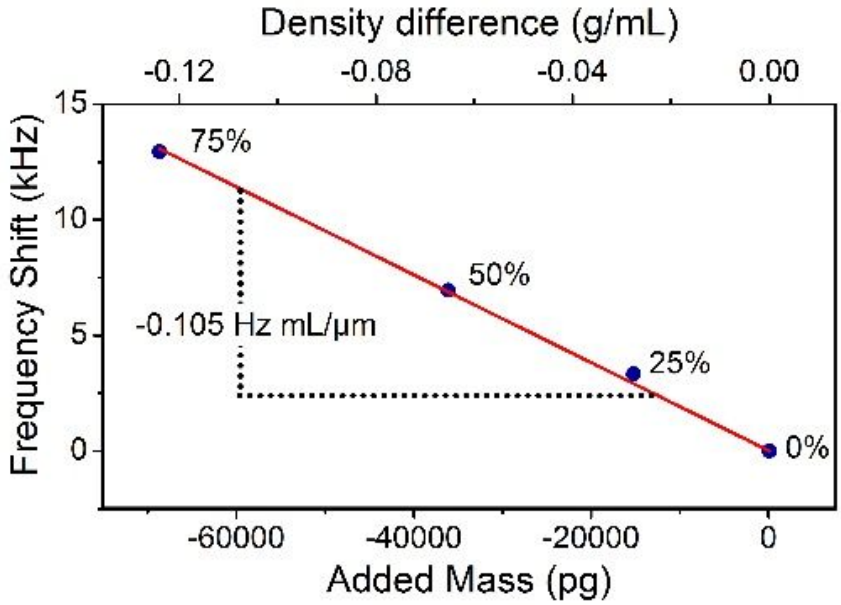

Figure S5. Mass calibration of the suspended device.

S4. Sensor Calibration: optical response

We have calibrated the refractive index responsivity by introducing a 50% aqueous glycerol solution. The microchannel is initially filled with ultra-pure water and the solution diffuses through all the resonator length within a time lapse of 2 minutes. This diffusion produces a continuous change in the solution concentration, from 0% to 50% glycerol, which results in a continuous change in the liquid's properties such as density and refractive index. The density change is measured in real time by measuring the frequency shift and after the calibration described in S3. Given the density of the solution, the concentration can be obtained by using mathematical models depicted in the literature[1]. Knowing the concentration, the refractive index is calculated from mathematical models found in previous works[2].

Our sensor exhibits a sinusoidal response to refractive index changes. The sensitivity to refractive index changes in the linear regions is of the order of 10^{-5}, Fig.S6.

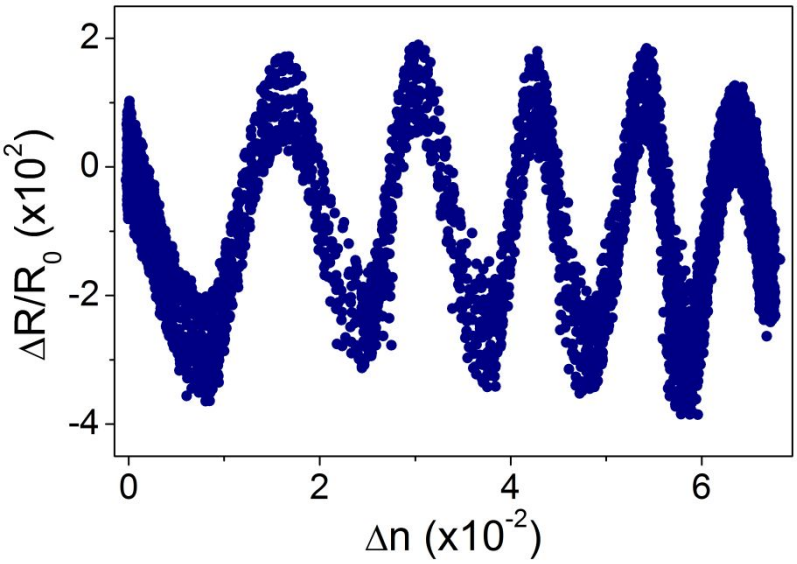

Figure S6. Sensor reflectance as a function of the refractive index in the inner liquid.

S5. Dynamic Characterization

In order to study the noise level and noise sources in our system, we depict in Fig. S7 the Allan deviation, $\sigma_{Allan}(\tau) = \sqrt{{\sigma_{Allan}}^2(\tau)}$, where ${\sigma_{Allan}}^2(\tau)$ is defined as the Allan variance and it is calculated from the average of frequency samples measured in a temporal integration time τ, ${\sigma_{Allan}}^2(\tau) = {}^{1}/_{2}\langle(\bar{f}(t+1) - \bar{f}(t))^2\rangle$. The mass resolution is calculated combining this Allan deviation and the mass responsivity obtained by the previous calibration described in S3. The Allan deviation reaches a value of 3×10^{-7} for an integration time of 0.15 s, which implies a mass resolution of 0.6 pg for this averaging time. For most of the measurements in this work we have chosen to acquire frequency data using an averaging time of 10 ms, which allows a higher particle flow rate (up to 20 particles per second) while keeping a good mass resolution (2 pg).)

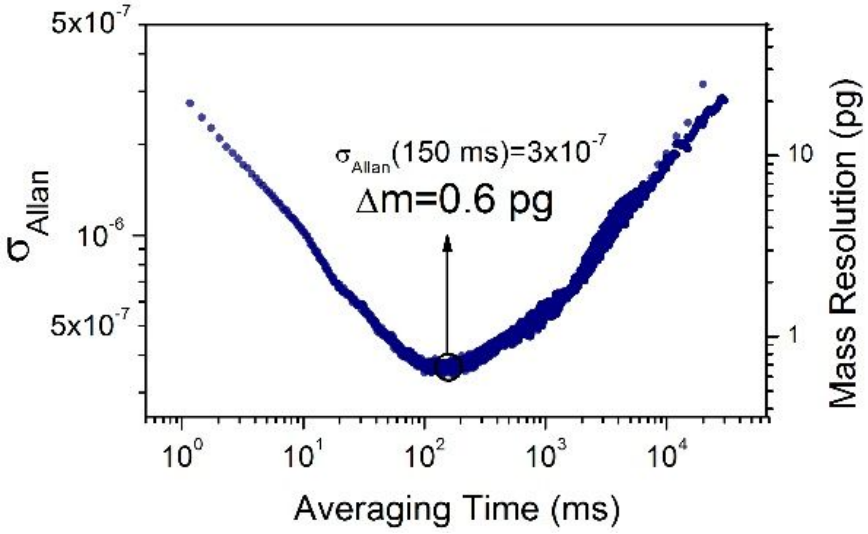

Figure S7. Experimental Characterization of the Allan variance of a representative capillary device.

S6. Single particles, dimers and particle aggregates

The combination of the mechanical and optical signal allows to split the contribution to the mechanical signal of individual particles when two (or more) particles flow through the capillary separated a distance shorter than the length of the suspended region of the resonator. As the particle passes through the resonator, it probes the mechanical modes, blue lines in Fig.S8, while the reflected power variation follows the laser gaussian profile (grey lines in Fig.S8). Thus, the optical signal is about 25 times faster than the mechanical signal for any flow speed (500 μm of suspended capillary versus 20 μm of laser spot size) as we can see in grey lines of Fig.S8. The optical signal informs of the time each particle passes under the center of the laser spot and hence, its position. Of course, we can only resolve particles separated a distance larger than the laser spot size. Previous works have addressed this problem tracking 2N flexural modes, being N the number of particles passing through the resonator simultaneously [3].

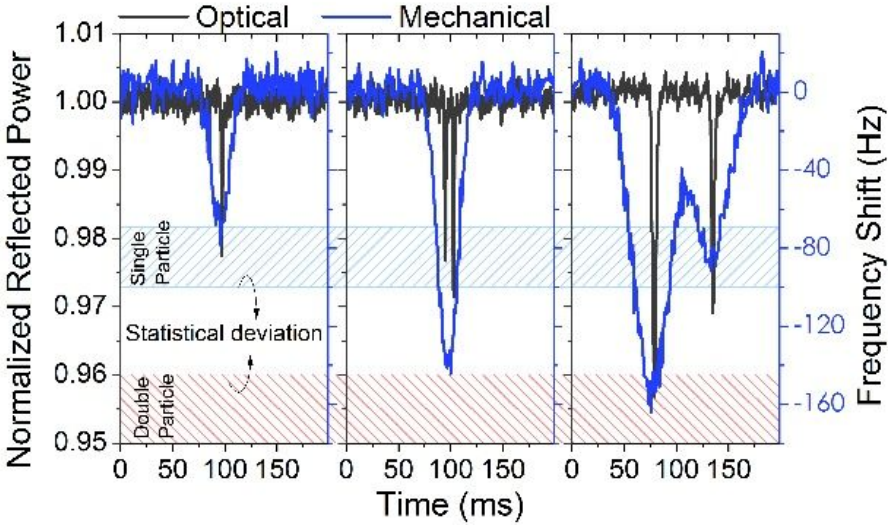

Figure S8. Experimental mechanical and optical real-time measurements of 8.4 μm silica particles. Left chart, single particle, middle chart, two particles passing through the capillary, right chart, two particles forming a dimer followed by a single particle. Since the optically sensitive area is smaller than the mechanically sensitive area, we can resolve particles separated a distance larger than the laser spot size.

Please, note that despite particles' clusters (dimers, etc.) are not discernible neither in the mechanical signal nor in the optical signal, they are easy to pinpoint if we regard to the mass distribution maxima, as they appear at integer multiples of the average mass of single particles, fig. S9.

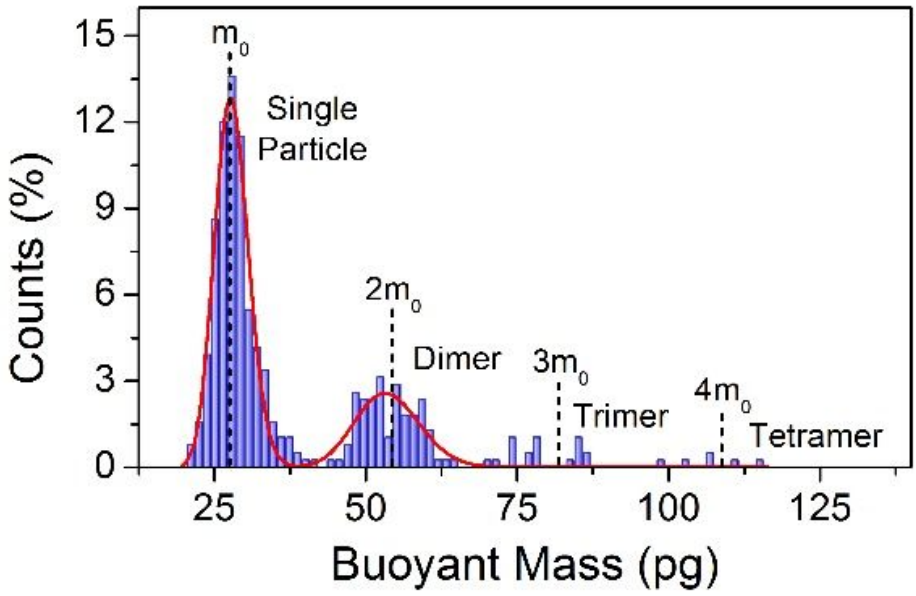

Figure S9. Mass distribution measured for 10 μm polystyrene microparticles (blue bars, N=383) and fit to a double buoyant mass distribution.

S7. Particle Morphological Characterization

For a better understanding of the data obtained by the mechano-optical measurements a sample of each population of microparticles was deposited on a silicon substrate in order to take SEM micrographs for measuring the size distributions (Fig S10).

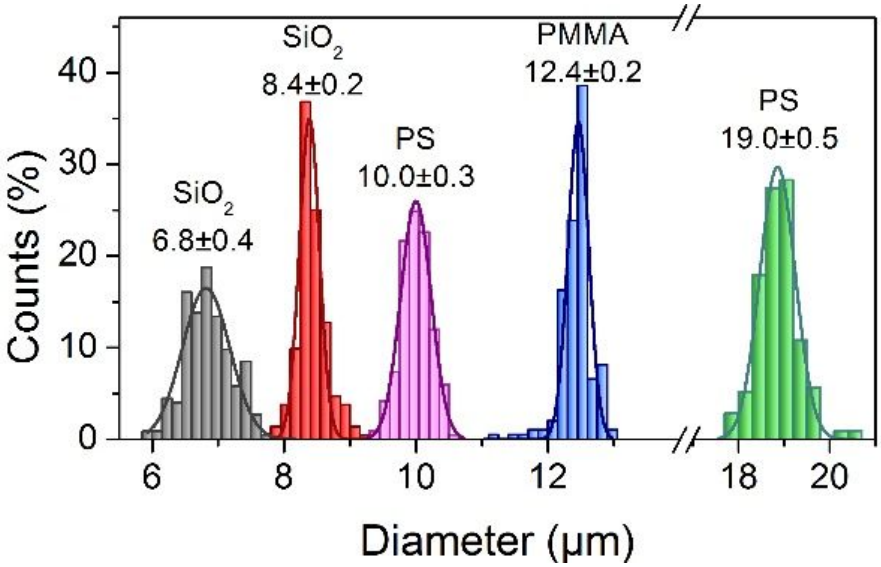

Fig S10: Size distributions of the 6.8 μm silica (gray bars, N=224), 8.4 μm silica (red bars, N=212), 10 μm polystyrene (magenta bars, N=217), 12.4 PMMA (blue bars, N=197=) and polystyrene 20 μm particles (green bars, N=212) by SEM micrograph.

S8. Cell Size Characterization

To obtain the size distribution of the measured cells, optical microscopy images were taken of MCF-10A and MCF-7 cells (Fig S11). Cells were cultured and suspended following the same procedure followed in the experiments with the devices and were placed on a petri plate that was immediately inspected under the microscope using a 10x objective. These measurements reveal an average diameter of 17±2 μm for the MCF-10A cells and 19±3 μm for the MCF-7 line.

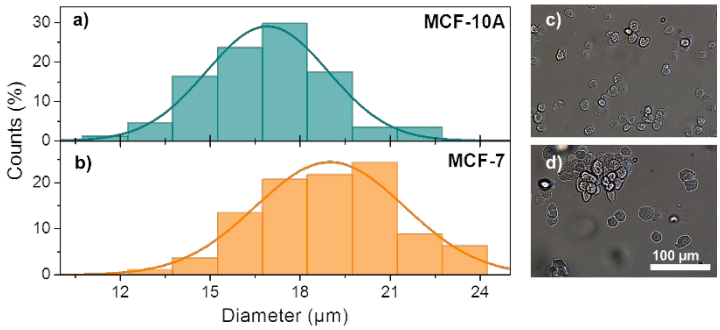

Figure S11: a) Size distribution measured (bin) and gaussian fit (line) of the MCF-10A cells (N=178) and b) MCF-7 cells (N=196). c) Optical Micrograph of MCF-10A cells and d) MCF-7.

S.9. FEM Simulations

The Finite Element Method (FEM) simulations were performed by using the commercially available software COMSOL Multiphysics, electromagnetic waves module. In order to decrease the computational costs, we have reduced the problem dimensionality to 2D, only simulating the cross section of the capillary. The domain calculation comprises the air, the upper wall of fused silica, water, the particle, the lower wall of fused silica, air, and reflective substrate of silicon. The materials and dimensions were taken to mimic the experimental conditions, next Fig. S12. The whole calculation domain is closed by a scattering boundary condition

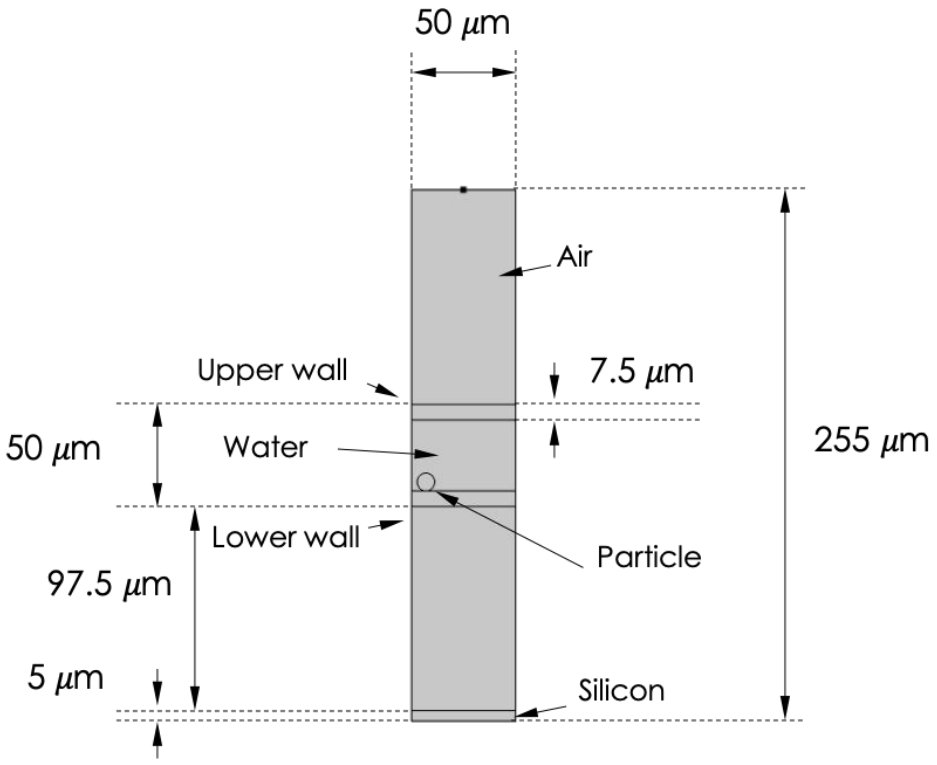

Figure S12: Calculation domain in FEM simulations.

In order to simulate the experiment, a gaussian beam is introduced as background field. We have parametrically displaced the particle and, for each point, calculate the propagation of the far field in the air, by using the well-known Straton-Chu formula. After that, we have integrated the propagated field over a sector angle of equal numerical aperture than the long working distance microscope used in the experiments. The maximum size of the elements in this calculation was set to 50 nm and the minimum 10 nm to keep the memory under control, which ends up with 2.5 M of elements for each calculation point.

References

1 Volk, A. & Kähler, C. J. J. E. i. F. Density model for aqueous glycerol solutions. **59**, 75, doi:10.1007/s00348-018-2527-y (2018).

2 Herráez, J. & Belda, R. *Refractive Indices, Densities and Excess Molar Volumes of Monoalcohols + Water*. Vol. 35 (2006).
3 Olcum, S., Cermak, N., Wasserman, S. C. & Manalis, S. R. High-speed multiple-mode mass-sensing resolves dynamic nanoscale mass distributions. *Nature Communications* **6**, 7070, doi:10.1038/ncomms8070 (2015).